JOURNAL OF THERMOPHYSICS AND HEAT TRANSFER
Vol. 12, No. 2, April–June 1998

Direct Simulation of High-Altitude Ultraviolet Emission from the Hydroxyl Radical

Koffi K. Kossi* and Iain D. Boyd†
Cornell University, Ithaca, New York 14853
and
Deborah A. Levin‡
Institute for Defense Analyses, Alexandria, Virginia 22331

Ultraviolet emissions radiated by hydroxyl (OH) are computed for hypersonic nonequilibrium flow conditions corresponding to the Bow-Shock Ultra-Violet-2 flight experiment. The flowfield is analyzed using the direct simulation Monte Carlo method. These computations include direct analysis of the electronically excited state of hydroxyl. Ultraviolet emission is estimated using a nonequilibrium radiation code. New algorithms are described that improve the numerical resolution of the excited state that occurs at number densities as low as 10^{-3} cm^{-3}. Results are presented for the altitude range from 80 to 100 km. It is shown that the high-altitude emission is sensitive to modeling of the interaction of the gas with the vehicle surface. Sensitivity of emission predictions to freestream concentrations of hydrogen-bearing species is also considered. It is found that the quasi-steady-state assumption often employed in the nonequilibrium radiation code is invalid at high altitude. Comparison of the predicted values for peak OH emission with flight measurements indicates good agreement. Detailed comparisons of the spectra, however, indicate that the simulations fail to include strong nonequilibrium effects observed in the measured data.

Nomenclature

A = excited electronic state designation or reaction rate constant, m^3 mol^{-1} s^{-1}
E = activation energy or electronic energy level, J
g = statistical weight
h = Planck's constant, 6.625×10^{-34}, J s
$\bar{h}$ = altitude, m
k = Boltzmann's constant, 1.38×10^{-23}, J K^{-1}
$\bar{k}$ = rate coefficient, m^3 mol^{-1} s^{-1}
M = third body species
N = species number of particles, temperature exponent in rate coefficient expression
n = species number density, m^{-3}
t = time, s
T_e = electronic temperature, K
T_r = rotational temperature, K
T_t = translational temperature, K
T_v = vibrational temperature, K
V = cell volume, m^3
W = particle weight
X = mole fraction
Z = distance from the body, m
ν = frequency, Hz
ρ = mass density, kg m^{-3}
τ = lifetime, s

Subscripts
diss = dissociation
ex = exchange
form = formation
qu = quenching
[ ] = concentration annotation

Superscripts
e = electronic index
i = particle index
r = rotation index
s = species index
t = translation index
v = vibration index
0, 1 = excited states index
∞ = initial condition

Introduction

A WIDE range of coupled physical phenomena occur in hypersonic flows about slender bodies including the rocket bow shock and its plume. The accurate prediction of the optical radiation emitted from these flows is difficult because of the complex coupling of many different physical phenomena. It is not uncommon for predictions of missile radiation signatures to be in error by orders of magnitude. To address this issue for the possible use of ultraviolet sensors, two flight experiments have been flown to measure radiation from the bow shock of a missile flying at 3.5 km/s (BSUV-1, Ref. 1) and 5.1 km/s (BSUV-2, Ref. 2). In a series of previous investigations,[1–5] generally successful computations of emissions caused by nitric oxide (NO) and atomic oxygen (O) have been obtained. In these prior studies, significant improvements were required in terms of physical models and numerical algorithms to achieve agreement with the flight data.

The present investigation continues these studies by consideration of data from BSUV-2 for emission from the hydroxyl radical (OH). An earlier study obtained qualitative results using continuum fluid dynamics for this data at altitudes below 88 km.[3] The study reported here, however, has the goal of breaking new ground by obtaining the first quantitative predictions of the OH radiation. The data for OH emission from BSUV-2 are only available at high altitudes (above 80 km).

Received Sept. 29, 1997; revision received Dec. 15, 1997; accepted for publication Dec. 16, 1997.

*Research Associate, Mechanical and Aerospace Engineering.
†Associate Professor, Mechanical and Aerospace Engineering. Member AIAA.
‡Research Staff Member, Science and Technology Division. Member AIAA.

Hence, all flowfield analyses are performed using the direct simulation Monte Carlo method (DSMC).

For prediction of emission, hydroxyl is a more attractive molecule than NO. In the first place, it has only one significant electronically excited state, the A state: OH(A). In addition, the rates of de-excitation of this molecule because of collision and spontaneous processes have been studied extensively in the laboratory. Thus, at the onset of the analysis, there are fewer unknown physical coefficients for the OH system in comparison to that for NO emission. Because of the relative simplicity of the OH system, it is a goal of the present study to include the production and quenching of the single excited state directly in the DSMC flowfield simulations. This will be found to require the development of special algorithms to allow adequate numerical resolution of the excited state that appears as a trace species.

In the following text a description is made of the numerical methods employed in this study. The physical models and numerical algorithms developed for the DSMC analysis are discussed. The nonequilibrium radiation code (NEQAIR) is also briefly described. In terms of results, a procedure for deriving low-altitude data from the BSUV-2 flight experiment is first discussed. General properties of the DSMC flowfield solutions are then presented. Direct comparison of the predicted peak emissions and spectra with the BSUV-2 data are provided. Finally, sensitivity of the predicted emission to various aspects of the simulations is discussed.

Numerical Methods

In this section the numerical methods employed in the present investigation are described. The physical models employed in the DSMC computations are first reviewed. Then, several new algorithms are introduced that improve simulation of reacting trace species. Finally, the nonequilibrium radiation code is briefly outlined.

DSMC Physical Models

The DSMC code employed in the present study is based on the vectorized algorithm described in Ref. 6. The code includes finite rates of rotational and vibrational relaxation, and dissociation, exchange, and recombination chemical reactions. A nine-species reacting flow model is employed for the following species: N_2, N, O_2, O, NO, and H_2O, OH, H, and the electronically excited state OH(A). In addition to the familiar air reactions, the hydrogenated species undergo the reactions listed in Table 1. The air chemistry is simulated using the dissociation and exchange reaction models described in Ref. 5. The reactions listed in Table 1 are modeled using the total collision energy form of the generalized collision energy model described in Ref. 4. A description of the approach employed to simulate the spontaneous de-excitation of OH(A) is given in the next section.

In a previous study[5] it was found that the prediction of ultraviolet emission for both NO and O was sensitive to the model assumed for interaction of the gas with the vehicle surface. In particular, the peak emission was found to vary by a factor of about 5 for modest variation in α_t, the accommodation coefficient for the translational energy mode. In Ref. 5, it was found that the best agreement of prediction with experimental data occurred for a value for α_t of 0.85. This value is consistent with molecular beam experiments. In the present study, the assumption of fully diffuse reflection (all accommodation coefficients are set to unity) is retained as the default. However, additional computations are performed for decreased accommodation coefficients. The surface temperature in all cases is taken as 500 K as measured during the BSUV-2 flight.

DSMC Trace Species Algorithms

For the flow conditions considered here, the mole fractions of N_2, O_2, and O are orders of magnitude higher than those for the other chemical species. To resolve trace species in the DSMC technique, a weighting scheme has been developed[7] that allows species with different mole fractions to be represented by similar numbers of particles in the simulation. This is achieved by assigning a numerical weight W_i to each particle i. The number density of species s in a particular cell is then given by

$$n_s = \Sigma_{N_s} / V \tag{1}$$

where N_s is the number of particles of species s in the cell that is of volume V. This weighting scheme was successfully applied to the prediction of NO emission for the BSUV-2 flight experiment as discussed in Ref. 5. In the present investigation the weighting scheme is needed to resolve the excited state OH(A) and its precursors, OH and H_2O. It will be found that OH(A) exists in the flows at number densities less than 10 cm^{-3}, and these are handled without difficulty by the weighting scheme.

Additional problems relating to the adequate resolution of OH(A) did occur in the study, however. For any OH(A) particle to exist in the flow, it must be produced through collisional excitation. It is important to note that only collisional excitation mechanisms for OH(A) production are considered in this study. For all conditions considered there are few intermolecular collisions and, therefore, the number of possible excitation events is small. Hence, the number of OH(A) particles in the simulation can be very low. This problem is addressed in two ways. First, whenever a collision involving an OH particle has sufficient energy to allow electronic excitation, the reaction probability is set to unity. The numerical weights of the products of this reactive collision are then adjusted to ensure conservation of mass. In addition, a special procedure is employed for these excitation collisions whereby several OH(A) particles are created (say, 30) instead of just one. Each OH(A) particle

Table 1 Rate coefficients for hydrogenated reactions

Reaction	Rate coefficient, $m^3\,mol^{-1}\,s^{-1}$, $\bar{k} = AT^N e^{(-E/kT)}$		
	A	N	E/k, K
$H_2O + N_2 \rightarrow OH + H + N_2$	5.81×10^{-15}	0.00	−53,000.0
$H_2O + O_2 \rightarrow OH + H + O_2$	1.13×10^{-7}	−1.31	−59,400.0
$H_2O + O \rightarrow OH + H + O$	1.13×10^{-7}	−1.31	−59,400.0
$OH + N_2 \rightarrow O + H + N_2$	1.25×10^{-15}	0.06	−51,000.0
$OH + O_2 \rightarrow O + H + O_2$	1.25×10^{-15}	0.06	−51,000.0
$OH + O \rightarrow O + H + O$	1.25×10^{-15}	0.06	−51,000.0
$H + O_2 \leftrightarrow OH + O$	3.65×10^{-16}	0.00	−8,450.0
$O + H_2O \leftrightarrow OH + OH$	1.13×10^{-16}	0.00	−9,240.0
$OH + N_2 \leftrightarrow OH(A) + N_2$	2.38×10^{-19}	0.40	−46,600.0
$OH + O_2 \leftrightarrow OH(A) + O_2$	6.75×10^{-18}	0.40	−46,600.0
Reaction	Einstein coefficient, s^{-1}	——	——
$OH(A) \rightarrow OH + h\nu$	1.44×10^{6}	——	——

has unique properties, but all are sampled statistically using the familiar DSMC procedures to conserve energy and momentum. The numerical weight of each particle is again adjusted to conserve total mass for consistency with Eq. (1).

Using these algorithms, it is possible to maintain several thousand OH(A) particles in the simulation even at the highest altitude condition. However, the following spontaneous de-excitation reaction can quickly remove all of these precious OH(A) particles:

$$\mathrm{OH}(A) \rightarrow \mathrm{OH} + h\nu \tag{2}$$

The rate of decrease of OH(A) caused by this process may be written

$$\frac{\mathrm{d}[\mathrm{OH}(A)]}{\mathrm{d}t} = -\frac{[\mathrm{OH}(A)]}{\tau} \tag{3}$$

where square brackets indicate number density, and $\tau = 6.9 \times 10^{-7}$ s is the excited-state lifetime. To first order, the number density of OH(A) at the end of a simulation time step Δt may be written

$$[\mathrm{OH}(A)]^{t+\Delta t} = [\mathrm{OH}(A)]^{t}[1 - (\Delta t/\tau)] \tag{4}$$

To incorporate this process into the DSMC computation, a constant de-excitation probability of $\Delta t/\tau$ is applied to every OH(A) particle every time step. For the time step employed in the 100-km computation, the de-excitation is most likely about 0.145. Hence, this mechanism can very rapidly depopulate the simulation of OH(A) particles. To address this difficulty a special procedure is implemented in which the numerical weight of each OH(A) particle is adjusted and no OH(A) particles are actually removed from the simulation. For consistency with Eq. (4), it may be shown from Eq. (1) that the numerical weight W of all OH(A) particles must be decreased according to

$$W^{t+\Delta t}_{\mathrm{OH}(A)} = W^{t}_{\mathrm{OH}(A)} \times [(1 - (\Delta t/\tau)] \tag{5}$$

The production of OH particles by Eq. (2) is performed statistically. Thus, for every OH(A) particle found in the flowfield, the probability of creating an OH particle with the same numerical weight is $\Delta t/\tau$.

Nonequilibrium Radiation Model

The nonequilibrium radiation code NEQAIR (Ref. 8) is employed for the prediction of ultraviolet emission from the DSMC flowfield solutions. The modeling of OH ultraviolet emission using NEQAIR is discussed and verified in Ref. 9. A common assumption made in using the NEQAIR code is that a quasi-steady-state (QSS) exists for the number densities of the electronically excited species. The assumption requires that the time scale of chemical processes is much smaller than the time scales for diffusion and for changes in overall properties.[8] Under these conditions the local values of temperatures and ground-state species number densities obtained from the DSMC computation may be used to compute the populations of the electronically excited states.

The present study departs from this approach by calculating directly in the DSMC computation the number density of OH(A). Because this species will be found to occur in very small quantities, inclusion of OH(A) in the computation does not affect the number density of OH to a significant extent. Hence, the present study allows direct assessment of the validity of the QSS assumption for high-altitude flows.

Experimental Data

Detailed spectral measurements from BSUV-2 are available from about 110 km to 71 km. However, information for the

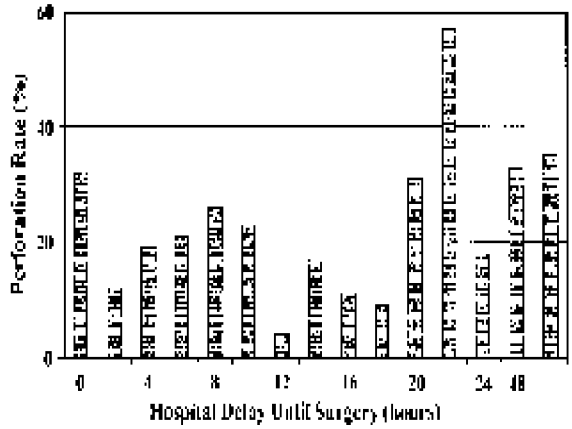

Fig. 1 Comparison of spectra measured on BSUV-2 as a function of altitude.

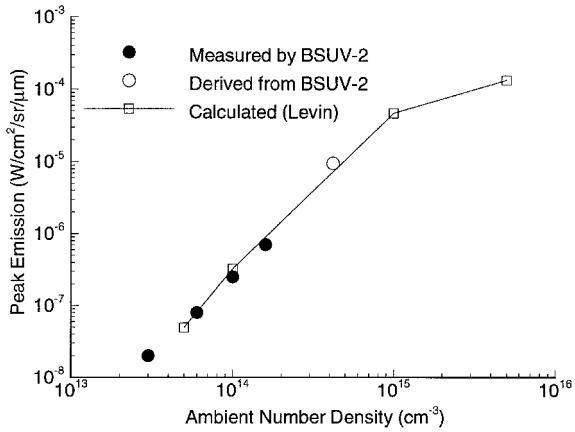

Fig. 2 Comparison of OH(0–0) spectral peak data and analytic kinetic model for derivation of data at 80 km.

OH system is only readily accessible for altitudes of 84 km and higher. At lower altitudes, the OH emission may be present but subsumed by the NO vibronic structure. This behavior is illustrated in Fig. 1 in which BSUV-2 spectra at three different altitudes are shown. Note how the OH(0–0) transition at 0.31 μm becomes apparent at the higher altitudes. In the following analysis, the idea is to extend the flight OH data to 80 km based on physical arguments. At this altitude, most of the OH in the flow originates through the dissociation of water. Hence, the flight data can be equated to the computed radiance at 80 km to determine the freestream water concentration. The derived water concentration can be checked for consistency with the available atmospheric data.

A comparison between the measured spectral peak heights of the OH(0–0) transition with the radiation calculated from a kinetic analysis was presented in an earlier work.[3] The results of this analysis are shown in Fig. 2. Closed-form density-dependent expressions were derived from the kinetic analysis by making two key assumptions. The first is that N_2–water dissociation is the dominant process in forming OH, i.e.,

$$\frac{\mathrm{d}[\mathrm{OH}]}{\mathrm{d}t} = k_{\mathrm{diss}}[\mathrm{H_2O}][\mathrm{N_2}] - k_{\mathrm{form}}[\mathrm{OH}][\mathrm{H}][\mathrm{N_2}] \tag{6}$$

where the square brackets indicate concentration, k_{diss} is the dissociation rate of water, and k_{form} is the formation rate. The second assumption is that the OH(A) lifetime τ is much less than flow and reaction times, thereby producing OH(A) in steady state with respect to the ground state. Hence

$$\frac{[\mathrm{OH}(A)]}{[\mathrm{OH}]} \approx \frac{k_{\mathrm{ex}}[\mathrm{N_2}]}{k_{\mathrm{qu}}[\mathrm{N_2}] + 1/\tau} \tag{7}$$

where k_{ex} and k_{qu} are the excitation and quenching rates, respectively. At high altitudes the chemical kinetics are far from steady state, so that

$$\frac{d[OH]}{dt} \neq 0 \approx k_{diss}[H_2O][N_2] \tag{8}$$

Because the collisional excitation rates are low

$$[OH(A)] \approx k_{ex}[N_2][OH(X)]\tau \tag{9}$$

This gives the result that at high altitudes (80 km and higher) the radiation [or the concentration of OH(A)] is proportional to density "cubed." Using this expression, a spectral peak height is derived at 80 km and is indicated in Fig. 2. Note that the OH(A) concentration calculated by either Eq. (8) or (9) is a close approximation to the QSS calculation performed in NEQAIR and discussed in the next section.

Using the DSMC flowfield and the full radiation model, the OH spectrum is computed at 80 km. An estimate of the ambient water mole fraction is then obtained through comparison of the peak with the derived 80-km data point. The derived water mole fraction is 1.5×10^{-6}. This value lies within the range of data reported in Ref. 10, which are adapted from Ref. 11 from atmospheric measurements and varying from about 1.0×10^{-6} to 8.0×10^{-6}.

Results

As in previous computational studies of the BSUV-2 flight, only flow over the 10-cm-radius spherical nose of the vehicle is simulated. In every case the velocity is 5.1 km/s, and four different altitudes are considered: 80, 88, 94, and 100 km. Freestream conditions are listed in Table 2. The concentrations of the hydrogenated species are obtained from a model atmosphere presented in Ref. 10. There is significant uncertainty in the determination of the composition of species involved in odd-hydrogen chemistry in the middle atmosphere. There can be important variations caused by geographic location and time in the solar cycle. In terms of water content the values listed in Table 2 represent an upper bound that occurs under conditions of solar minimum. There are no measurements of OH concentration above 70 km in the literature. Hence, the values employed here from the model atmosphere are considered representative rather than definitive.

The presentation of results is divided into two sections: (1) variation of general flow properties over the altitude range of interest, and (2) comparison of predicted emission with BSUV-2 flight data including sensitivity of predicted emission to gas–surface interaction model and freestream composition.

General Flow Properties

In Figs. 3a and 3b, profiles of number densities and temperatures along the stagnation streamline of the vehicle are shown for the 80-km case. A well-defined shock is formed with significant excitation of the rotational and vibrational modes. Sufficient chemistry occurs such that the number density of OH rises above that of H_2O close to the surface. The peak number density of OH(A) is about 10^6 cm^{-3}. In Fig. 3b, the electronic temperature of OH is computed from the predicted populations of the ground state (n_0) and first excited state (n_1) using

$$T_e = -\frac{E_1/k}{\log[(g_0/g_1)(n_1/n_0)]}$$

where E_1 is the energy of the first electronic excited state. Note that the electronic temperature computed in this manner is significantly higher than the vibrational temperature.

The effect of rarefaction on this flow may be seen in Figs. 4a and 4b, which show number densities and temperatures along the stagnation streamline at an altitude of 100 km. Note that for clarity of the results presentation, the shock-layer domain is reduced in Fig. 4. This explains the fact that the temperatures do not reach the initial value. In this case, there are significant reductions in the peak temperatures for all three energy modes. There is very little chemistry and all species have a relatively flat density profile indicating the importance of diffusion. This is also indicated by the peak number density of OH(A) of about 10^{-3} cm^{-3} for this case.

To assess the QSS assumption generally employed in the nonequilibrium radiation analysis, profiles of OH(A) along the stagnation streamline are shown in Figs. 5a and 5b for altitudes of 80 and 100 km, respectively. Once again, for clarity, the shock-layer domain is reduced in Fig. 5b. The profile labeled

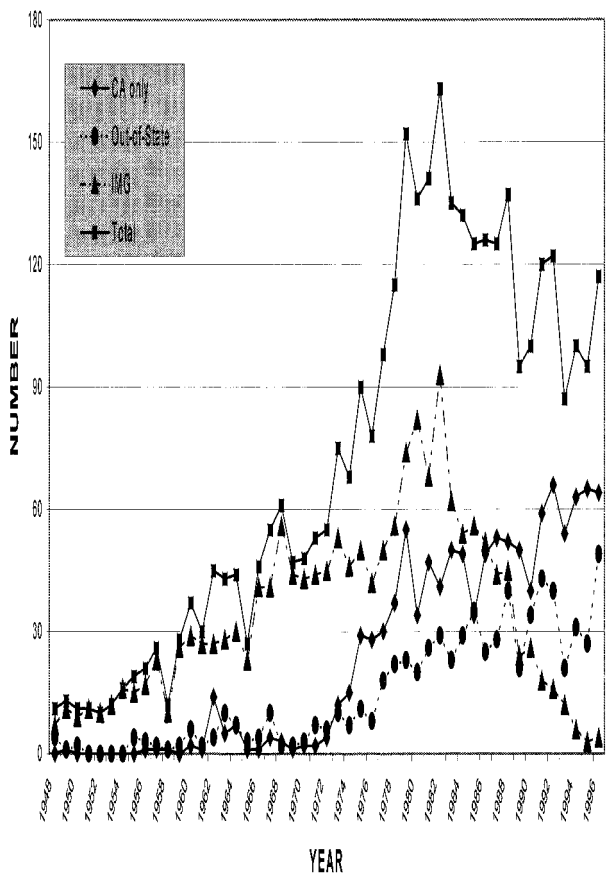

Fig. 3 a) Number densities and b) temperatures along the stagnation streamline at 80 km altitude.

Table 2 Flow conditions

$\bar{h}$, km	ρ_∞, kg m^{-3}	T_∞, K	X_{H_2O}	X_{OH}	X_H
80	2.00×10^{-5}	181	5.6×10^{-6}	4.3×10^{-9}	2.0×10^{-7}
88	5.11×10^{-6}	195	3.0×10^{-6}	1.2×10^{-9}	7.0×10^{-6}
94	1.30×10^{-6}	177	1.2×10^{-6}	3.0×10^{-10}	9.0×10^{-6}
100	5.68×10^{-7}	185	7.2×10^{-7}	2.0×10^{-10}	1.0×10^{-5}

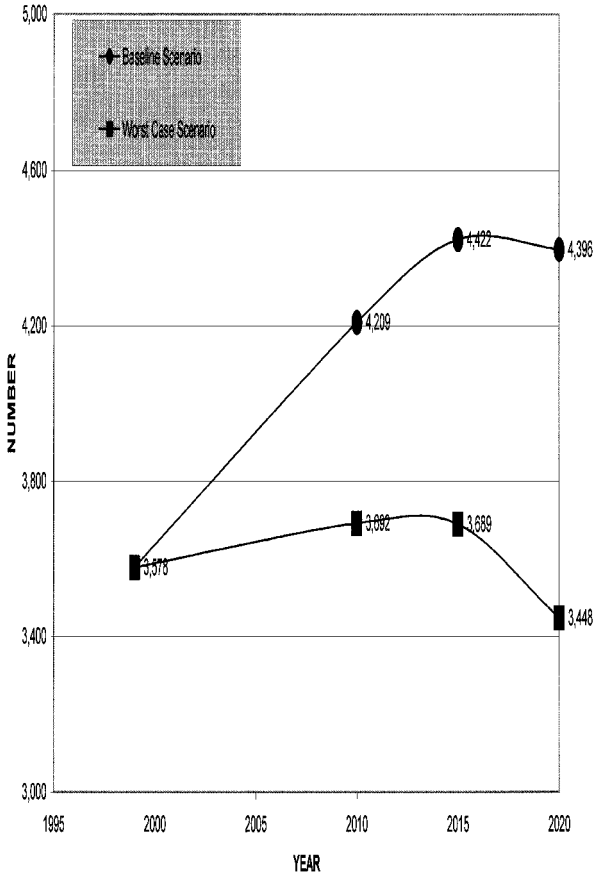

Fig. 4 a) Number densities and b) temperatures along the stagnation streamline at 100 km altitude.

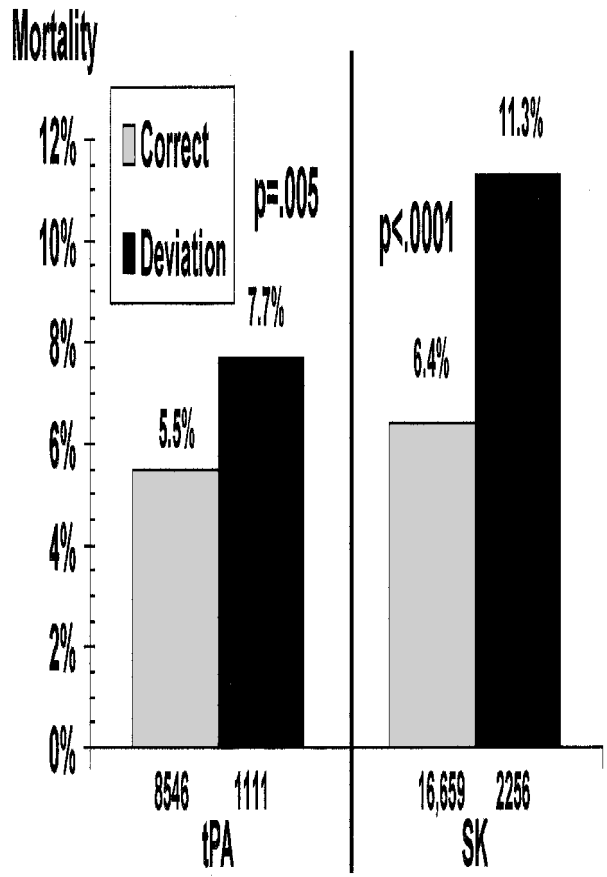

Fig. 5 Variation in OH(A) concentration along the stagnation streamline at a) 80 and b) 100 km altitudes.

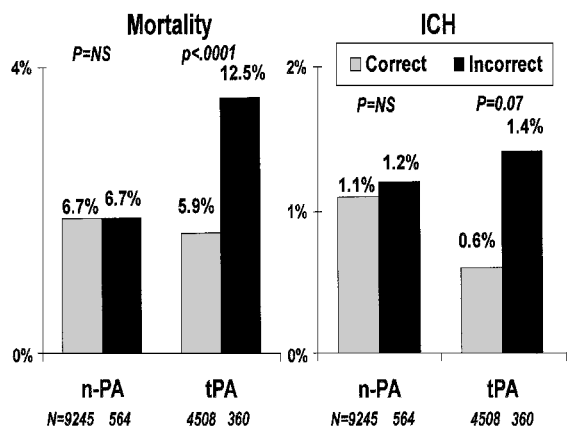

Fig. 6 Peak emission at 0.31 μm as a function of altitude.

QSS uses the DSMC solution in each cell along the stagnation streamline for temperatures and all species number densities {except [OH(A)]} to compute the OH(A) profile. Clearly, at 80 km, there is sufficient collision activity to make the QSS assumption quite reasonable. The OH(A) is formed by neutral collisional excitation of OH in the ground electronic state by molecular nitrogen and oxygen. Further, the relatively high collision rate in this flow prevents the OH(A) molecules from diffusing. The agreement between the DSMC and QSS profiles is satisfactory.

By contrast, at 100 km, the DSMC profile for OH(A) is nearly flat, indicating that diffusion processes dominate over collisional excitations. The sharp decrease in [OH(A)] predicted by the QSS assumption at the vehicle wall (Z = −0.1016 m) is because of the reduction of translational temperature as predicted by the DSMC computation. The direct simulation of OH excitation shows no such decrease because OH(A) molecules diffuse all along the stagnation streamlines from their point of formation because of the reduced collision rate under this condition. Assuming that the DSMC technique predicts the diffusive phenomena accurately, the emissions shown next are all computed using the OH(A) profiles provided by the direct simulations rather than using those obtained from the QSS approximation.

Emission Predictions

Several data sets for the peak emission at 0.31 μm as a function of altitude are compared in Fig. 6. Experimental data are taken from the spectra measured on the BSUV-2 flight. For these data, the background NO emission is subtracted to leave a component owing only to OH. As discussed earlier, a data point at 80 km is derived from the flight data because the OH features there are supposed to be subsumed by emission from NO. Two different sets of computational results are provided. The results labeled $\alpha = 1$ use the freestream concentrations for H_2O, OH, and H listed in Table 2, and the gas–surface interaction is modeled using fully diffuse reflection. This profile provides good agreement with the flight data up to about 88 km. In this range, the predicted emission lies within a factor of 2 of the flight data. This disagreement falls well within the range of uncertainty in specification of the freestream atmospheric compositions of the hydrogen compounds. Above 88 km, the $\alpha = 1$ predictions lie below the flight data by several orders of magnitude.

To assess the sensitivity of these predictions, further computational studies are performed. In the calculations labeled $\alpha < 1$ in Fig. 6, energy accommodation coefficients less than unity are employed. Specifically, the coefficients for the translational, rotational, and vibrational modes are set to $\alpha_t = 0.85$, $\alpha_r = 0.5$, and $\alpha_v = 0.1$, respectively. The accommodation coefficient for the translational mode used here is consistent with values observed in molecular beam experiments. It is also necessary to

note that the values of the accommodation coefficients of the internal energy modes do not influence the radiation prediction. The freestream composition is again that listed in Table 2. Use of this gas–surface interaction model, which has been partially verified in Ref. 5 through comparison with the NO and O BSUV-2 data, leads to significant increases (factors of orders of magnitude) in the predicted emission. At all altitudes, the DSMC results using the modified gas–surface interaction model are now in excellent agreement (within a factor of 4) with the flight data. The explanation for the increases in emission is partly illustrated in Figs. 7a and 7b, which compare the temperature and OH(*A*) number density profiles along the stagnation streamline computed at 100 km for the two different approaches to gas–surface interaction. When the accommodation coefficients are less than unity, the resulting translational temperature is increased in comparison to the case in which perfectly diffuse reflection is assumed. In addition, with a translational energy accommodation coefficient less than unity, the OH(*A*) number density is increased significantly.

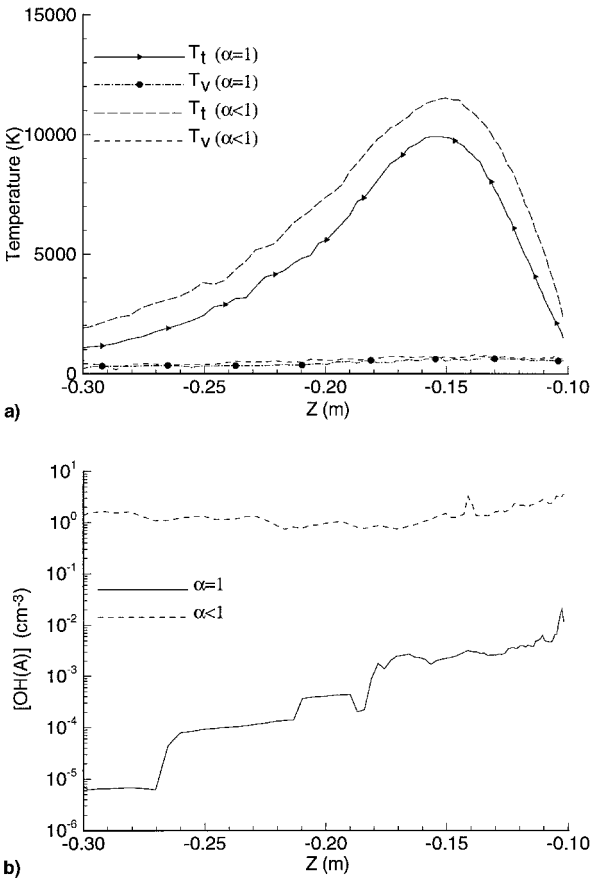

Fig. 7 a) Temperatures and b) OH(*A*) concentration along the stagnation streamline at 100 km altitude.

A more complete understanding of these differences requires consideration of collision energies rather than temperatures. When complete accommodation is assumed, the highest energy collision in the flow is between an incident freestream molecule traveling at 5 km/s and a reflected particle traveling at a typical speed of 1 km/s. The collision energy of this interaction is barely above the activation energy for the electronic excitation of OH. In contrast, when incomplete accommodation is assumed, the peak collision energy occurs for interaction between incident and reflected particles both traveling at 5 km/s (in opposite directions), and this impact energy is significantly above the activation energy.

Sensitivity of the emission predictions to the assumed freestream concentrations is also considered. The freestream concentrations for H_2O and H are again those listed in Table 2. In the case of OH, the concentration is obtained from a model atmosphere presented in Ref. 12. Comparison of these values with the model data of Ref. 10 is shown in Fig. 8. The difference between the models represents an attempt to quantify the uncertainty in determining the freestream concentration of hydroxyl at high altitude. The flowfield is computed using the $\alpha < 1$ parameters, and the emission results are compared with the BSUV-2 data in Fig. 9. At lower altitudes the computed emission is most sensitive to the freestream water composition, indicating that the primary source of OH here is through the dissociation of H_2O. However, at high altitudes, the emission is almost directly proportional to the freestream mole fraction assumed for OH. At all altitudes the DSMC results are in very good agreement with the flight data within a factor of 3, except at 100 km where the peak emission is decreased by a factor of 3 with respect to the decrease of an OH mole fraction at that altitude with the model data of Ref. 12.

While it is satisfying to obtain reasonable predictions of the peak height, it is also of interest to consider the full spectra. In Figs. 10a and 10b, spectra computed using the $\alpha = 1$ parameters are compared with the BSUV-2 data at altitudes of 88 and 100 km. Note that the nonequilibrium radiation computations only consider the spectral contributions from OH. All other contributions, notably those from NO, are omitted for clarity. In both cases, the computed spectra do not reproduce many of the important spectral features of the data. This inconsistency was observed in earlier calculations as well.[9] The calculated spectra do not predict the presence of the OH(*A*)1–0 vibronic transition at 0.28 μm and the shoulder of the 0–0 peak at 0.31 μm is too narrow. Both of these features are absent from the simulated spectra because the predictions for the OH rotational and vibrational temperatures are inaccurate. For the cases considered here, these temperatures for OH are almost identical to the in-

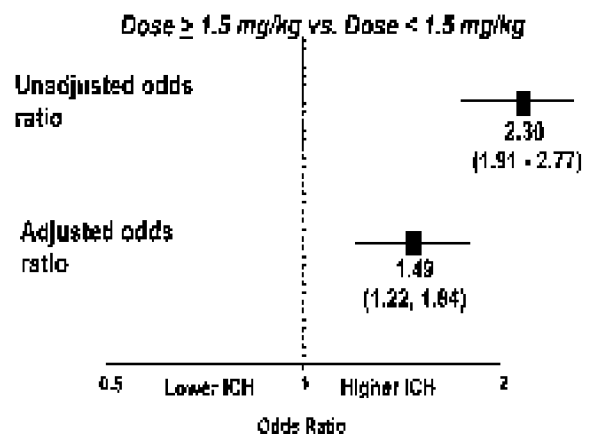

Fig. 8 Variation with altitude of the atmospheric composition of hydroxyl.

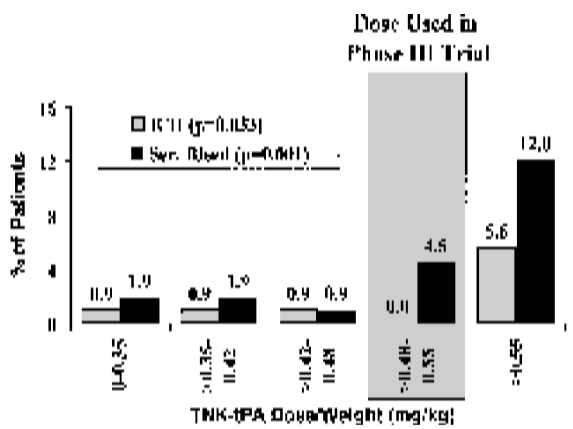

Fig. 9 Peak emission at 0.31 μm as a function of altitude.

Fig. 10 Ultraviolet spectra: a) at 88 km altitude and b) normalized at 100 km.

ternal energy temperatures for the bulk gas. Figure 4b shows bulk vibrational and rotational temperatures on the order of 1000 K, whereas the spectral data indicate the OH vibrational and rotational temperatures to be on the order of 7000 and 3000 K respectively, as shown in Ref. 9. This large discrepancy cannot be explained in terms of thermal relaxation effects. It is proposed that OH molecules that are both rotationally and vibrationally excited must be formed through the dissociation of water. Detailed molecular dynamics analysis of water dissociation appears to confirm this idea.[13]

Summary and Conclusions

The DSMC was applied to compute formation of the single electronically excited state of hydroxyl, OH(A), in a nonequilibrium, hypersonic flow. The conditions considered correspond to the BSUV-2 flight experiment over the altitude range of 80–100 km. Numerical resolution of the excited state, which appears as a trace species through rare chemical reactions, required the development of several new algorithms. The new schemes were successful in resolving OH(A) at number densities as low as 10^{-3} cm^{-3}.

Comparisons of the number density profiles of OH(A) computed directly in the DSMC analysis exhibited a significantly diffusive behavior, particularly at the higher altitudes. This indicated that the QSS assumption often employed in nonequilibrium radiation modeling was not applicable under these conditions.

The profiles of OH(A) computed directly by the DSMC method were used to obtain ultraviolet spectra. When surface accommodation coefficients of 1 were used for all energy modes, the spectral peaks predicted at 0.31 μm were in good agreement with the BSUV-2 flight data below 88 km. At higher altitudes, the predictions were lower than the measurements by orders of magnitude. It was found that the computed emission was sensitive to the model employed in the DSMC computation for the interaction between the gas and vehicle surface. When accommodation coefficients less than unity were employed the emission increased significantly. Using coefficients obtained from a previous study and freestream concentrations of H_2O and OH taken from the literature the predicted peak emissions at all altitudes agreed with the BSUV-2 data within a factor of 4. The present study also demonstrated that the high-altitude-predicted emission was sensitive to the assumed freestream concentration of hydroxyl.

Comparison of the spectral shapes predicted in this study with data measured on BSUV-2 showed relatively poor agreement. While the peak of the OH(0–0) transition was accurately predicted, all other features observed in the flight data were missing from the predicted results. This indicated that the gas was in a much more highly nonequilibrium state than predicted by the simulation. This shows that additional research is needed to study, in detail, the dynamics by which OH is formed through the dissociation of water.

Acknowledgments

The work performed at Cornell was funded by the U.S. Air Force Office of Scientific Research under Grant F49620-96-1-0091. Work performed at the Institute for Defense Analyses was carried out for the U.S. Air Force Office of Scientific Research in coordination with the Innovative Science and Technology Office of the Ballistic Missile Defense Organization.

References

[1]Erdman, P. W., Zipf, E. C., Espy, P., Howlett, L. C., Levin, D. A., Loda, R., Collins, R. J., and Candler, G. V., "Flight Measurements of Low-Velocity Bow Shock Ultraviolet Radiation," *Journal of Thermophysics and Heat Transfer*, Vol. 7, No. 1, 1993, pp. 37–41.

[2]Erdman, P. W., Zipf, E. C., Espy, P., Howlett, L. C., Levin, D. A., Collins, R. J., and Candler, G. V., "Measurements of Ultraviolet Radiation from a 5-km/sec Bow Shock," *Journal of Thermophysics and Heat Transfer*, Vol. 8, No. 3, 1994, pp. 441–446.

[3]Levin, D. A., Collins, R. J., Candler, G. V., Wright, M. J., and Erdmann, P. W., "Examination of OH Ultraviolet Radiation from Shock-Heated Air," *Journal of Thermophsyics and Heat Transfer*, Vol. 10, No. 2, 1996, pp. 200–208.

[4]Boyd, I. D., Bose, D., and Candler, G. V., "Monte Carlo Modeling of Nitric Oxide Formation Based on Quasi-Classical Trajectory Calculations," *Physics of Fluids*, Vol. 9, 1997, pp. 1162–1170.

[5]Boyd, I. D., Phillips, W. D., and Levin, D. A., "Prediction of Ultraviolet Radiation in Nonequilibrium Hypersonic Bow-Shock Waves," *Journal of Thermophysics and Heat Transfer*, Vol. 12, No. 1, 1998, pp. 38–44.

[6]Boyd, I. D., and Gokcen, T., "Computation of Axisymmetric and Ionized Hypersonic Flows Using Particle and Continuum Methods," *AIAA Journal*, Vol. 32, 1994, pp. 1828–1837.

[7]Boyd, I. D., "Conservative Species Weighting Scheme for the Direct Simulation Monte Carlo Method," *Journal of Thermophysics and Heat Transfer*, Vol. 10, No. 4, 1996, pp. 579–585.

[8]Park, C., "Calculation of Nonequilibrium Radiation in the Flight Regimes of Aero-Assisted Orbital Transfer Vehicles," *Thermal Design of Aero-Assisted Orbital Transfer Vehicles*, edited by H. F. Nelson, Vol. 96, Progress in Astronautics and Aeronautics, AIAA, New York, 1985.

[9]Levin, D. A., Laux, C., and Kruger, C., "A General Model for the Spectral Calculation of OH Radiation in the Ultraviolet," *Journal of Quantitative Spectroscopy and Radiative Transport* (submitted for publication).

[10]Brasseur, G., and Solomon, S., *Aeronomy of the Middle Atmosphere*, 2nd ed., Reidel Publishers, Dordrecht, The Netherlands, 1986, pp. 442, 443.

[11]Solomon, S., Crutzen, P. J., and Roble, R. G., "Photochemical Coupling Between the Thermosphere and the Lower Atmosphere. I. Odd Nitrogen from 50 to 120 km," *Journal of Geophysics*, Vol. 87, 1982, p. 7206.

[12]Shimazaki, T., *Minor Constituents in the Middle Atmosphere*, 1st ed., Reidel Publishers, Dordrecht, The Netherlands, 1985, p. 169.

[13]Nyman, G., Rynefors, K., and Holmlid, L., "Energy Distributions from Decomposition of a Complex $H_2O \rightarrow OH + H$ on a Simplified Potential Energy Surface, as a Function of Total Angular Momentum: Comparison Between Classical Trajectories and an RKKM-Type Statistical Simulation," *Chemical Physics*, Vol. 134, 1989, pp. 355–373.